


Article

Insights into Adsorption of Chlorobenzene in High Silica MFI and FAU Zeolites Gained from Chromatographic and Diffractometric Techniques

Luisa Pasti ^{1,*}, Elisa Rodeghero ², Giada Beltrami ², Matteo Ardit ², Elena Sarti ¹, Tatiana Chenet ¹, Claudia Stevanin ¹ and Annalisa Martucci ^{2,*} 

¹ Department of Chemistry and Pharmaceutical Sciences, University of Ferrara, Via L. Borsari 46, 44121 Ferrara, Italy; elena.sarti@unife.it (E.S.); tatiana.chenet@unife.it (T.C.); claudia.stevanin@unife.it (C.S.)

² Department of Physics and Earth Sciences, University of Ferrara, Via Saragat 1, 44122 Ferrara, Italy; elisa.rodeghero@unife.it (E.R.); giada.beltrami@unife.it (G.B.); rdtmtt@unife.it (M.A.)

* Correspondence: psu@unife.it (L.P.); mrs@unife.it (A.M.); Tel.: +39-0532-455346 (L.P.); +39-0532-974730 (A.M.)

Received: 9 January 2018; Accepted: 19 February 2018; Published: 26 February 2018

Abstract: In this work, the capability of two commercial high silica zeolites (HSZs), namely ZSM-5 and Y, for the removal of chlorobenzene (CB) from water was investigated by combining chromatographic and diffractometric techniques. The adsorption isotherms and kinetics of CB on ZSM-5 and Y zeolites were determined from batch tests. The adsorption kinetics were very fast; the time to reach equilibrium was less than 10 min. The equilibrium data of CB on the two HSZs showed dissimilarities that are particularly evident in the adsorption data concerning the low concentration range, where Y zeolite is characterized by low adsorption. On the contrary, at higher solution concentrations the adsorption capacity of Y is higher than that of ZSM-5. The crystalline structures of Y and ZSM-5 saturated with CB were investigated by X-ray diffraction (XRD) techniques. Rietveld refinement analyses of XRD data allowed for quantitative probing of the structural modifications of both zeolites after CB adsorption and provided insight into the preferred zeolite adsorption sites in both microporous materials. The refined framework–extraframework bond distances confirm that interactions between the selected organic contaminant and hydrophobic zeolites are mediated via co-adsorbed H₂O. The occurrence of H₂O–CB–framework oxygen oligomers explains variations in both the unit cell parameters and the shape of the channels, clearly confirming that water plays a very relevant role in controlling the diffusion and adsorption processes in hydrophobic zeolites.

Keywords: chlorobenzene; sorption; ZSM-5; X-ray powder diffraction; Rietveld structure refinement; chromatography

1. Introduction

Industrial and agricultural discharges, chlorine disinfection by-products (DBPs) of drinking water and wastewater, and incineration of wastes are the main sources of chlorine and organochlorine compounds (OCICs), such as chlorobenzene (CB). These compounds can cause toxic effects on both human health and environmental systems, even at low concentration [1]. In particular, the Environmental Protection Agency (EPA) fixed the maximum contaminant level (MCL) of CB at 0.1 mg/L; above this threshold value CB can cause negative health effects, such as gastrointestinal irritations, hepatotoxicity and kidney damages [2]. Therefore, it is important to remove this pollutant from the environment and different methodologies have been proposed.

Actually, the physical method based on adsorption processes is a recuperative method exploited for in situ water treatments which combines high flexibility of the system, efficiency even at low

concentration levels, low energy, cheap operating costs, and possible waste reductions [3]. Different adsorbent materials can be employed, and their efficiency depends on the host-guest interactions between sorbent and sorbate [4–13]. In general, carbonaceous adsorbents are low cost materials, widely employed in remediation technology. However, their applicability can be limited by fouling that cause a pore blocking (i.e., to the presence of dissolved organic matter), to low adsorption capacity, sharp rise of bed temperature and difficulty of regeneration [14–17]. In recent years, organic contaminants removal by single-walled carbon nanotubes (SWCNTs) has attracted great interest due to their chemical, electronic and mechanical properties [18]. However, the saturation capacity of these adsorbents for OCICs is moderate and functional groups on the surface of carbonaceous adsorbents can further reduce the adsorption features [19–21]. In the past few decades, surfactant modified clays have been proposed as a potential alternative to carbonaceous adsorbents for removing OCIC pollutants. Indeed, it has been proved that these materials are efficient and they can be easily regenerated. One of the main disadvantages is their limited stability due to a progressive release of surfactant which can have a negative impact on biota [22–25]. Synthetic and hydrophobic zeolites offer an attractive and efficient option for the removal of chlorine, and organochlorine compounds from water. The main advantages are related to their high surface area and porous structure, high specific capacity and organic pollutants selectivity. Additionally, fast kinetics, mechanical, biological and chemical stability make them promising and efficient adsorbents [4,6–8,26–28]. Furthermore, their high thermal stability guarantees the possibility of regeneration through thermal treatments in order to reintroduce them in new adsorption processes [5,29–33].

This work is part of a wider study aimed at systematically evaluating the adsorptive capacity of high silica zeolites (HSZ) (e.g., mordenite, ZSM-5, faujasite, beta, ferrierite [4,7,10,29,30]) for fuel-based compounds differing in chemical properties (e.g., polarity, functional groups, size, host-guest interactions, etc.), which can provide useful information to accurately predict the behavior of HSZs as well as improve their individual performance.

The objective of this study is to evaluate the capability of two commercial HSZs, ZSM-5 (MFI topology), and Y zeolite (FAU topology) [34], for removal of chlorobenzene (CB) from water. For that purpose, the adsorption process from water was investigated in order to gain information on the interactions between the selected organic contaminant and hydrophobic zeolites. The information gathered from this work provides a tool for the selection of adsorbent materials for environmental remediation. Additionally, the investigation of host-guest interactions can provide information on the fate and transport of OCICs in the environment, and in particular for the partition of those contaminants in the mineral fraction of soils, normally constituted by aluminosilicate.

2. Experimental Methods

2.1. Materials and Methods

High-silica Y (code HSZ-390HUA, 200 SiO₂/Al₂O₃ molar ratio, 750 m²/g surface area, 0.05 wt % Na₂O content) and ZSM-5 (code CBV 28014, 280 SiO₂/Al₂O₃ molar ratio, 400 m²/g surface area, 0.01 wt % Na₂O content) hydrophobic zeolites were purchased in their as-synthesized form by Tosoh Corporation (Tokyo, Japan) and Zeolyst International (Conshohocken, PA, USA) respectively.

Chlorobenzene (CB) in its anhydrous form (purity of 99.8%) was provided by Sigma-Aldrich (Steinheim, Germany) and used as received.

2.2. Batch Adsorption

The adsorption isotherm was determined using the batch method. Batch experiments were carried out in duplicate in 20 mL crimp top reaction glass flasks sealed with PTFE septa (Supelco, Bellefonte, PA, USA). The flasks were filled in order to have the minimum headspace and a solid:solution ratio of 1:2 (mg·mL⁻¹) was employed. After equilibration, for 24 h at a temperature of 25.3 ± 0.5 °C under

stirring, the solids were separated from the aqueous solution using centrifugation (14,000 rpm for 30 min).

The concentration of contaminants in the aqueous solution, before and after the contact with the adsorbent was determined by Headspace Gas Chromatography coupled to Mass Spectrometry (HS-GC-MS). The analysis was carried out using an Agilent GC-MS system (Santa Clara, CA, USA) consisting of a GC 6850 Series II Network coupled to a Pal G6500-CTC injector and a Mass Selective Detector 5973 Network.

HS autosampler injector conditions are: incubation oven temperature 80 °C, incubation time 50 min, headspace syringe temperature 85 °C, agitation speed 250 rpm, agitation on time 30 s, agitation off time 5 s, injection volume 500 µL, fill speed 30 µL·s⁻¹, syringe pull-up delay 5 s, injection speed 250 µL·s⁻¹, pre-injection delay 0 s, post injection delay 2 s, syringe flush 30 s with nitrogen. A DB-624 UI GC column (L = 20 m, I.D. = 0.18 mm, df = 1.00 µm film thickness, Agilent, Santa Clara, CA, USA) was used. High purity helium was the carrier gas with a constant flow rate of 0.7 mL·min⁻¹. The oven temperature gradient started at 40 °C for 4 min and then ramped to 130 °C at 15 °C·min⁻¹. The injector temperature was kept at 150 °C. All samples were injected in split mode (10:1). The mass spectrometer operated in electron impact mode (positive ion, 70 eV). The source temperature and the quadrupole temperature were set to 230 °C and 150 °C, respectively. The mass spectra were acquired in full scan mode. The electronic scan speed was 1562 amu·s⁻¹ in a mass range from 30 to 300 amu. For identification and quantification of the target analyte the SIM (selected ion monitoring) chromatograms were extracted from the acquired signal by selecting the most abundant characteristic fragments at $m/z = 112$. Chromatographic peak of analytes was identified by comparison of the retention time and the mass spectrum with standard compound and library data; quantitative analysis was performed using calibration curves.

2.3. Thermal Analyses

The Netzsch STA 409 PC LUXX[®] (Gerätebau, Germany) simultaneous TG/DTA thermogravimetric balance was employed in order to carry out both thermogravimetric (TG) and differential thermal analyses (DTA) on Y and ZSM-5 zeolites before and after CB loading. The measurements were performed in constant air flux conditions using a heating rate of 10 °C/min, from room temperature (RT) to 900 °C.

2.4. X-ray Powder Diffraction Data Collection and Refinement Strategy

X-ray diffraction patterns on powders of Y and ZSM-5 zeolites loaded with CB were carried out on a Bruker D8 Advance (Karlsruhe, Germany) diffractometer (Cu K $\alpha_{1,2}$ radiation) equipped with a Sol-X detector. Diffraction data were collected at RT, in 3°–110° 2 θ (for ZSM-5) and 3°–100° 2 θ (for Y zeolite) 2 θ ranges respectively, with a counting time of 12 s each 0.02° 2 θ . Figure S1 reported observed, calculated and difference X-ray powder diffraction patterns of Y–CB (a) and ZSM-5–CB (b), respectively.

GSAS software [35] and the EXPGUI graphical interface [36] were employed for Y–CB and ZSM-5–CB structural refinements through a full profile Rietveld analysis. Unit-cell and structural parameters were determined starting from the monoclinic $P2_1/n$ (for ZSM-5) and the cubic $Fd-3$ (for Y) space groups of Martucci et al. [10], and Braschi et al. [11] structural models, respectively. The Bragg peak profiles were modelled by a Pseudo-Voigt function with 0.001% cut-off peak intensity. Refined coefficients were: two Gaussian terms (i.e., the $\tan^2\theta$ dependent GU and the θ independent GW), and two Lorentzian terms (i.e., $\cos\theta^{-1}$ dependent LX, $\tan\theta$ dependent LY), respectively. A Chebyshev polynomial function with 24 and 22 coefficients was used in order to empirically fit the instrumental background for Y and ZSM-5, respectively. In both structural refinements, scale factor, 2 θ -zero shift and unit-cell parameters were also refined. Soft constraints were initially imposed on Si–O, O–O, C–C and C–Cl bond distances (tolerance (σ) value of 0.04 Å) and completely removed in the final cycles. Finally, atomic coordinates, site occupancy and isotropic atomic displacement parameters were

refined. Furthermore, the displacement parameters for a given atom type were constrained to be equivalent (i.e., Si and O sites), thus limiting the number of refined atomic displacement parameters to two. Additionally, in Y-CB x/a and y/b parameters of the chlorobenzene molecule were constrained to be equal in order to maintain the planarity. Table 1 reports the details of the data collection and Rietveld refinements. In Supplementary Materials (Tables S1 and S2, respectively) the refined atomic coordinates, occupancies and isotropic thermal parameters of Y and ZSM-5 loaded structures are reported. Extraframework atomic fractional coordinates, thermal isotropic displacement factor and occupancy of Y-CB and ZSM-5-CB are in Tables S3 and S4, respectively. Selected bond distances (Å) and angles (°) within both the Y-CB and ZSM-5-CB framework and extraframework atoms are listed in Tables S5 and S6, respectively. CIFs for all reported crystal structures are added in Supplementary Materials as supplementary information.

Table 1. Details of the data collection and Rietveld refinements.

Parameter	ZSM-5	ZSM-5-CB	Y	Y-CB
	[Si ₉₆ O ₁₉₂]	[Si ₉₆ O ₁₉₂]·6(C ₆ H ₅ Cl)·8(H ₂ O)	[Si ₁₉₂ O ₃₈₄]	[Si ₁₉₂ O ₃₈₄]·32(C ₆ H ₅ Cl)·70(H ₂ O)
Space group	<i>P</i> 2 ₁ / <i>n</i>	<i>P</i> 2 ₁ / <i>n</i>	<i>Fd</i> -3 <i>m</i>	<i>Fd</i> -3
<i>a</i> (Å)	19.899(5)	19.919(1)	24.259(1)	24.263(1)
<i>b</i> (Å)	20.117(6)	20.107(1)	24.259(1)	24.263(1)
<i>c</i> (Å)	13.389(4)	13.3967(1)	24.259(1)	24.263(1)
α (°)	90	90	90	90
β (°)	90.546(3)	90.528(3)	90	90
γ (°)	90	90	90	90
<i>V</i> (Å ³)	5359.9(3)	5365.7(5)	14,277.1(1)	14,284.4(6)
Wavelength (Å): Cu K α ₁	1.540593	1.540593	1.540593	1.540593
Cu K α ₂	1.544427	1.544427	1.544427	1.544427
Refined 2 θ (°) range	3°–110°	3°–110°	3°–100°	3°–100°
Contributing reflections	5861	6362	620	620
<i>N</i> _{obs}	5350	5350	4850	4850
<i>N</i> _{var}	289	301	40	40
<i>R</i> _{wp} (%)	10.3	13.3	12.8	12.9
<i>R</i> _p (%)	9.4	10.4	12.5	12.6
<i>R</i> _F ² (%)	7.00	7.25	9.95	10.0

$R_p = \sum |Y_{io} - Y_{ic}| / \sum Y_{io}$; $R_{wp} = [\sum w_i (Y_{io} - Y_{ic})^2 / \sum w_i Y_{io}^2]^{0.5}$; $R_F^2 = \sum |F_o^2 - F_c^2| / |F_o^2|$

3. Results and Discussion

3.1. Adsorption Isotherms from Aqueous Solutions

The uptake q (mg·g^{−1}) was calculated as follows:

$$q = \frac{(C_0 - C)V}{m} \quad (1)$$

where C_0 is the initial concentrations in solution (mg·L^{−1}), C is the concentration at time t in kinetics experiments (mg·L^{−1}), V is the solution volume (L) and m is the mass of sorbent (g). In Figure 1 the uptake data for CB on Y and ZSM-5 are reported.

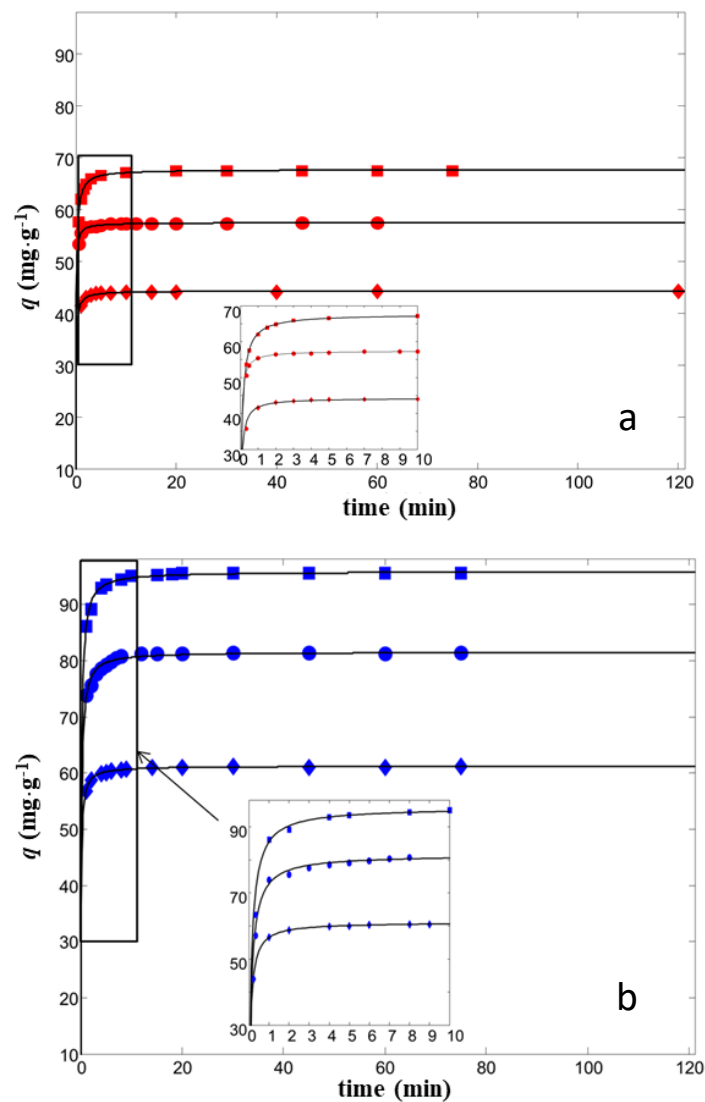


Figure 1. Chlorobenzene (CB) uptake vs. contact time for ZSM-5 (a) and Y (b) for initial concentration of 35, 25, 15 mg/L. The insets: enlarged image of the boxed regions.

It can be seen that the kinetics of the adsorption process was very fast; the equilibrium was reached in about 10 min. Similar behaviors were also observed for the adsorption of other aqueous contaminants, such as dichloroethane and toluene onto ZSM-5 and Y zeolites [5–10,13].

We have previously verified [5–10,13] that uptake data of the investigated zeolites can be fitted by the pseudo-second order model as:

$$q_t = \frac{k_2 q_e^2 t}{1 + k_2 q_e t} \quad (2)$$

where q_t and q_e are the amounts of solute adsorbed per mass of sorbent at time t and at equilibrium, respectively, and k_2 is the second-order adsorption rate constant. The values of equilibrium uptake q_e and the adsorption rate constant k_2 were obtained from non-linear fit of q_t vs. t (see Table 2). Analogous to what was observed for the adsorption of other aqueous contaminants, the uptake data of CB can be modelled by a pseudo-second order kinetic model, as indicated from the high coefficient of determination.

Table 2. Estimated kinetics parameters (see Equation (2)). The confidence limits at 95% of probability of the estimated parameters are reported in brackets.

	C_0 (mg·L ⁻¹)	q_t (mg·g ⁻¹)	k_2 (g·L ⁻¹ ·mg ⁻¹)	R^2
ZSM-5	15	23.4 (23.3, 23.5)	0.44 (0.41, 0.47)	0.9845
	25	44.3 (44.2, 44.3)	0.37 (0.33, 0.41)	0.9803
	35	67.6 (67.5, 67.6)	0.21 (0.19, 0.23)	0.9985
Y	25	39.3 (39.2, 39.4)	0.14 (0.11, 0.17)	0.9822
	35	70.3 (70.2, 70.3)	0.13 (0.11, 0.15)	0.9969
	45	82.3 (82.4, 82.5)	0.10 (0.085, 0.12)	0.9935

Furthermore, for the adsorption of CB it can be noted that the kinetic constant decreases by increasing the initial concentration [37], and that the adsorption onto Y zeolites is characterized by a lower kinetic constant than that found for ZSM-5. These findings allow us to generalize the difference observed in the adsorption kinetics of these two zeolites. In particular, the adsorption kinetics of neutral organic molecules (namely, toluene, dichloroethane, methyl tert-butylether and CB), which differ from each other in physicochemical properties and molecular dimensions, is faster on ZSM-5 than on Y zeolite.

It has been already shown that adsorption of organics in aqueous solutions onto ZSM-5 hydrophobic zeolites are well fitted by the Langmuir equation [5,6,8,13], that assumes monolayer adsorption onto energetically equivalent adsorption sites and negligible sorbate–sorbate interactions. The relationships describing the Langmuir isotherm is [38]:

$$q = \frac{q_s b C_e}{1 + b C_e} \quad (3)$$

where b is the binding constant (L·mg⁻¹) and q_s is the saturation capacity of the adsorbent material (mg·g⁻¹). The experimental data obtained for the adsorption of CB on both ZSM-5 and Y are shown in Figure 2. It can be observed that the isotherms are shaped differently from each other; they can be classified as concave (Type I) and sigmoidal (Type V) isotherms, respectively.

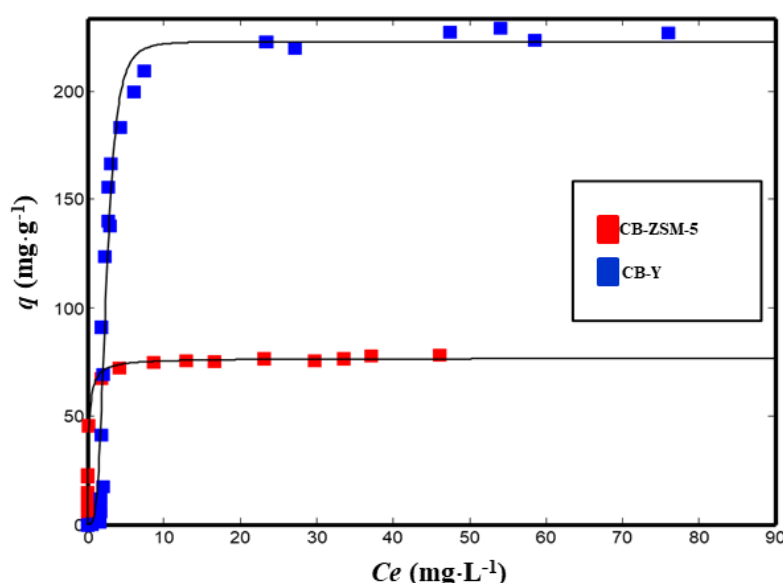


Figure 2. Adsorption isotherms of CB for ZSM-5 (red squares) and Y (blue squares).

Similar differences in the adsorption of polar organic compound from aqueous solution onto ZSM-5 and Y were also observed for methyl tert-butylether and toluene. In such cases, a Hill isotherm model was employed:

$$q_e = q_s \frac{c_e^n}{K_H + c_e^n} \quad (4)$$

where K_H is the Hill constant, and n is the Hill coefficient which is related to the degree of cooperativity. The Hill isotherm is often employed to describe cooperative adsorption in biological systems, and it has also been used to model adsorption data on zeolites due to evidence of the presence of water-organic compound clusters [39] inside the zeolite frameworks. Since the tendency to form clusters increases by increasing the porosity dimensions, the clusters are more probably formed in the large cage of Y than in the channel system of ZSM-5 [40]. To evaluate if clusters can be formed for CB, a structural investigation was carried out (vide infra).

In Table 3, the isotherm parameters for ZSM-5 and Y estimated by non linear fitting of Equations (3) and (4) respectively, are reported. It can be seen that the saturation capacity of these zeolites are higher than those obtained with graphite materials (i.e., 28.3 mg/g for dichlorobenzene) [41], and in particular Y zeolite has a saturation value higher than adsorbents single-walled carbon nanotubes, especially if they are partially oxidized [42]. In addition HSZs can be regenerated without significant loss of their adsorption properties [5,6,29,30]. Therefore hydrophobic zeolites are very promising adsorbents for the removal of chlorinated aromatic compounds from water.

Table 3. Isotherm parameters for the adsorption of CB on ZSM-5 and Y. SSE: sum of squared errors.

			R^2	SSE
Langmuir				
CB-ZSM-5	q_s	76.6 (74.8, 79.5)	0.9874	198
	b	5.0 (3.7, 6.6)		
Hill				
CB-Y	q_s	227 (218, 245)	0.9654	2135
	K_H	9.2 (6.6, 12.1)		
	n	5.5 (4.3, 6.7)		

3.2. Structural Modifications upon Chlorobenzene Adsorption on High Silica Zeolites

3.2.1. Y-CB

Y zeolite (FAU framework topology [34]) is built up of large cavities (α cages or supercages) with a diameter of 12 Å linked to four other supercages through 12 membered-ring windows (diameter of 7.4 Å) and cuboctahedral β cages connected each other through double hexagonal rings (D6R). Topological symmetry of the unloaded material is cubic $Fd-3m$, but it has been highlighted that the embedding of organic compounds can decrease the symmetry to $Fd-3$ [10–13,43]. A careful examination of powder diffraction patterns after chlorobenzene adsorption highlights that Y-CB peak positions are quite similar to those of the as-synthesized material in all the 2θ range investigated. Contrariwise, peak intensities strongly decrease after pollutant incorporation, especially at low 2θ angles (Figure 3).

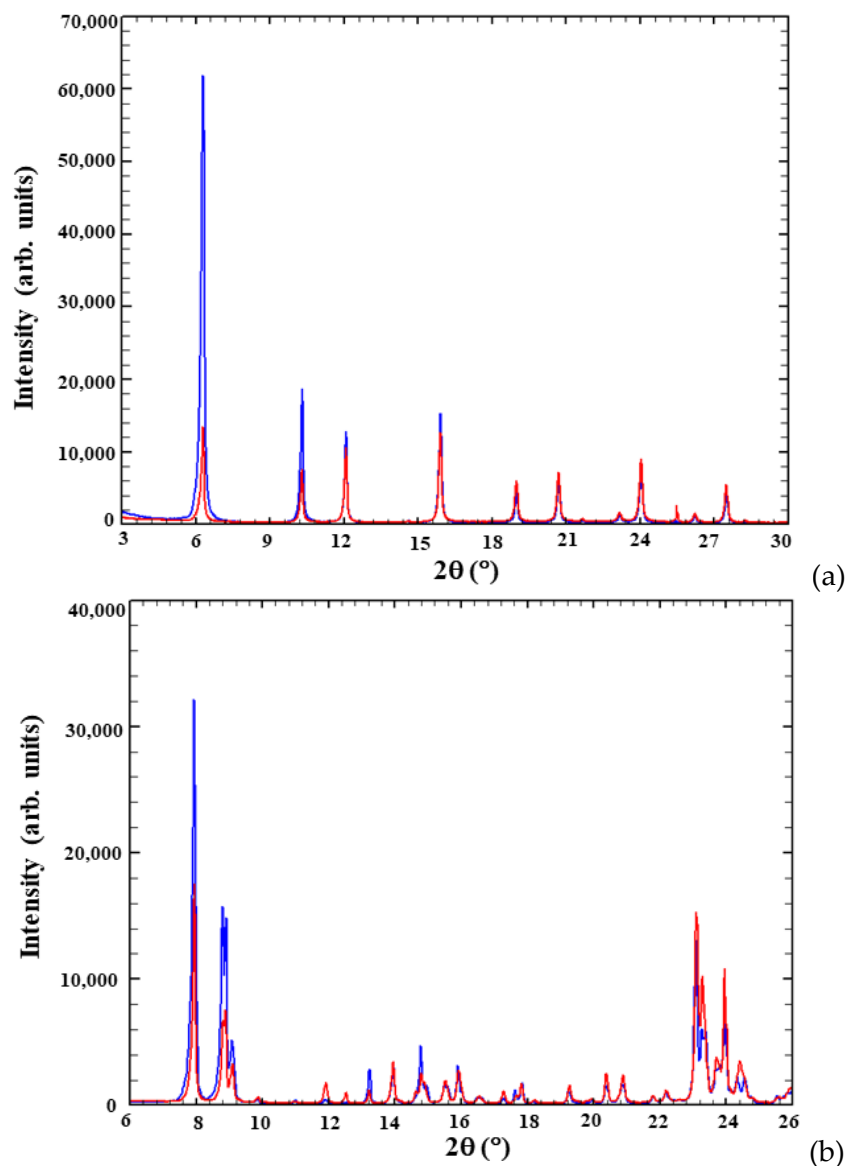


Figure 3. Observed powder diffraction patterns of Y-CB (a) and ZSM-5-CB (b), respectively, showing differences both in intensity and position of the diffraction peaks in the low and intermediate 2θ regions. Blue lines represent the unloaded samples, red lines the loaded ones.

These differences suggest variations in the extraframework species content as well as in the lattice parameters (Table 1), thus attesting to CB adsorption into the porous structure of the zeolite. After adsorption, the T1–O and T2–O mean distances are 1.621 and 1.620 Å, respectively, the O–T–O angles range from 103.3° to 112.3° (Table S5). The T–O–T bond angles adopt a wide range of values from 125° to 171° (mean value = 142°). The T–O, T–O–T and O–T–O grand mean values (Table S5) are in high agreement with those reported for other pure silica zeolites (PSZ) [44]. Furthermore, after adsorption the channel ellipticity ε (defined as the ratio between the smaller and larger O–O “free diameters” of the 12-rings) changed ($\varepsilon = 1.02$ in Y, $\varepsilon = 1.21$ in Y-CB) and at the same time, the openings reached a wider Crystallographic Free Area (C.F.A., sensu Baerlocher [34]) when compared with the as-synthesised material (Table 4), thus confirming the high flexibility of FAU-type materials [45,46].

Table 4. Crystallographic Free Area and ellipticity (ϵ) comparison between unloaded Y [11] and Y-CB systems. C.F.A. = $\pi \cdot (\text{mean radius})^2$ (\AA^2); ϵ = ratio between the longest and the shortest pore dimensions.

Parameter	Y-CB	Y [11]
O4–O4 distance (\AA)	11.16	9.81
O1–O1 distance (\AA)	9.68	9.70
Free diameter O4–O4 (\AA)	8.46	7.11
Free diameter O1–O1 (\AA)	6.98	7.00
Mean diameter (\AA)	7.72	7.06
Mean radius (\AA)	3.86	3.53
C.F.A. (\AA^2)	46.81	39.07
ϵ	1.21	1.01

Rietveld structural refinement allows us to detect 32 CB molecules per unit cell (corresponding to ~22.0% dry weight, dw %) located within the Y supercage (Figure 4a). Chlorobenzene molecules occupy one crystallographic independent and partially occupied site (C and Cl atoms in Table S3), and statistically can assume six different orientations (Figure 4a).

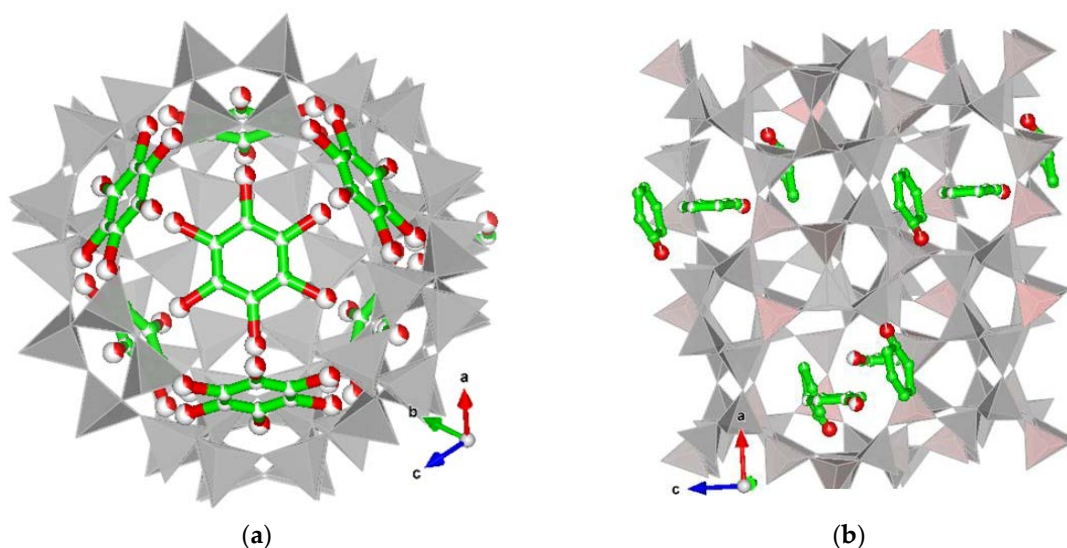


Figure 4. Distribution of CB molecules in Y (a) and ZSM-5 (b) zeolites, respectively. Chlorine (red circle) and carbon (green circle) are shown. Drawings produced by VESTA 3 [47].

Moreover, the evidence of relatively short Cl–O1 bond distances (i.e., Cl–O1 = 2.723(1) \AA and 2.680 \AA , respectively) proves that chlorobenzene directly interacts with framework oxygens.

Furthermore, difference-Fourier maps of the electron density analysis revealed the presence of co-adsorbed H_2O molecules hosted in three additional extraframework sites (W1, W2 and W3 sites, respectively, Table S3). Additionally, based on the W sites refined distance these sites interact with both each other and chlorine atoms forming oligomers (W2–W2 = 2.93 \AA , W3–Cl = 3.21 \AA and W1–W2 = 2.93 and 2.74 \AA , respectively) that strongly interact with the framework oxygen atoms via chlorine (Figure 4a). According to the recent literature [5–8,10–13,29,44], the strong interactions among organic molecules– H_2O short chain-frameworks play a relevant role in stabilizing the guest structures within the zeolite porosity.

On a whole, on the basis of Rietveld refinement 70 H_2O molecules (~8% dw %) were detected in good agreement with the TG curve (Figure 5a), which shows two main weight losses: the first one (about 7.3 dw % zeolite, 25–110 $^\circ\text{C}$) is related to desorption of species retained on the surface, the second one (23.5 dw % zeolite, 110–900 $^\circ\text{C}$) to the removal from the structure of loaded CB and H_2O molecules.

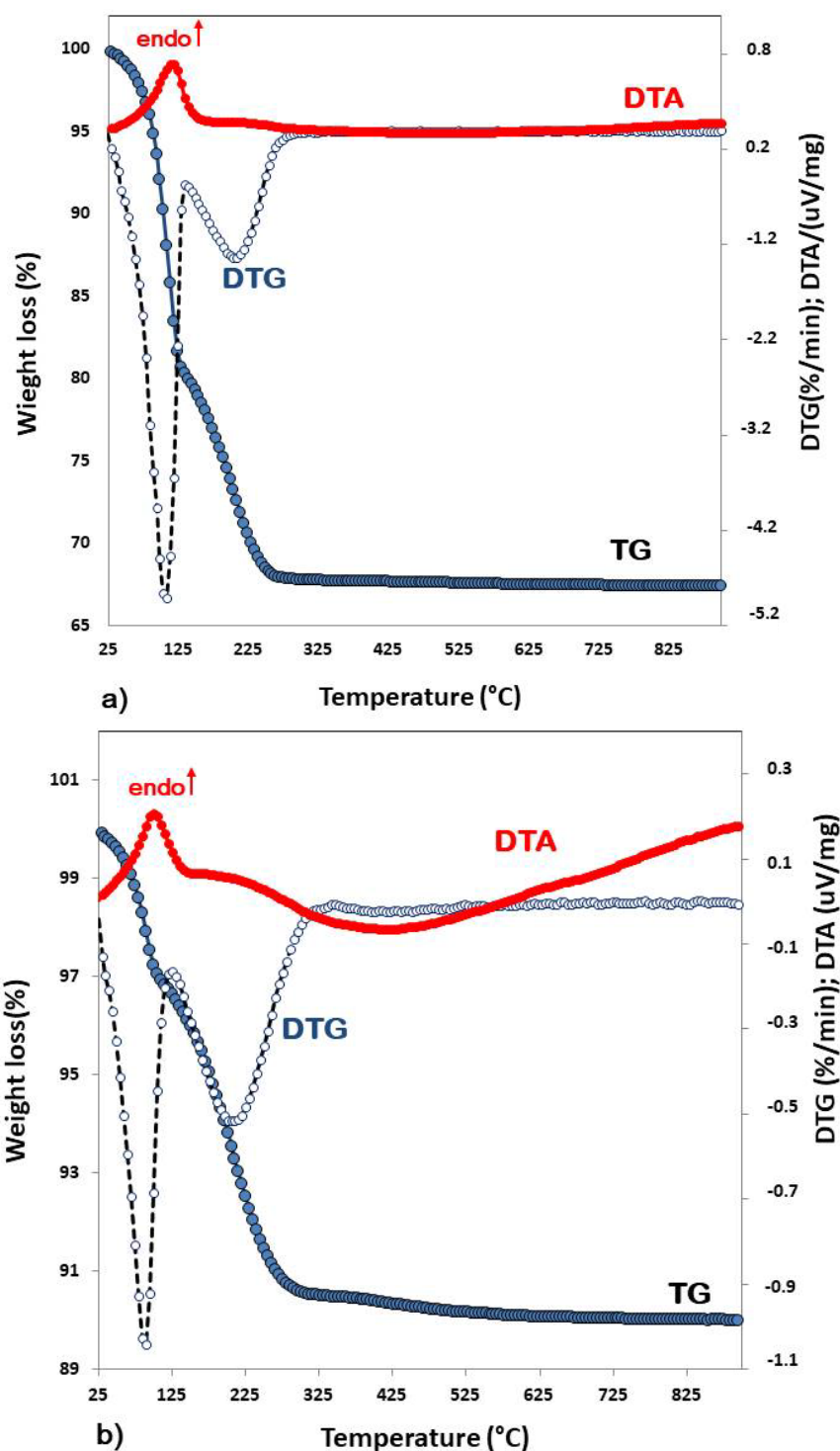


Figure 5. Thermal analysis of Y (a) and ZSM-5 (b) loaded with chlorobenzene from room temperature to 900 °C. In blue and gray circles, the total weight loss curve (TG) and the derivative of it (DTG); in red the differential thermal analysis (DTA) curve.

3.2.2. ZSM-5-CB

The ZSM-5 zeolite framework consists of two intersecting channel systems: a straight channel parallel to [010] direction and a sinusoidal one parallel to [100] direction [34]. Both channels are limited by 10MR of TO_4 tetrahedra with free diameters of 5.4–5.6 Å and 5.1–5.5 Å for sinusoidal and straight channel, respectively. After CB adsorption, the evolution of the powder diffraction pattern

indicates that ZSM-5 maintains its crystallinity as well as the monoclinic $P2_1/n$ symmetry. In Table 1, the comparison between refined lattice parameters of starting material and of the ZSM-5–CB system highlights the occurrence of chlorobenzene adsorption in the ZSM-5 micropores. The structural characterization was carried out starting with the model proposed by Rodeghero et al. [6] and an examination of the difference Fourier maps of the electron density suggested the presence of extraframework content. In detail, some of recognized maxima were reasonably attributed to chlorobenzene adsorption sites in both the sinusoidal channel (CB2 sites) and the intersection between sinusoidal and straight channels (CB1 sites) (Table S4, Figure 4b). On the whole, a total amount of about 6 molecules per unit cell (p.u.c.) of organics were detected. Besides, residual maxima of difference Fourier maps also indicate the presence of co-adsorbed H₂O molecules (~1.5 dw %) hosted at W1 and W2 sites. In particular, based on the refined distances between the extraframework content and framework oxygen atoms strong interactions among chlorobenzene molecules hosted in both adsorption sites (CB1 and CB2), H₂O molecules (W1 and W2 sites), and framework oxygen atoms occur (i.e., O4–C10 = 3.01(1) Å, O18–C9 = 2.61(1) Å, O31–C11 = 2.69(1) Å, O47–C11 = 2.99(1) Å, W2–W2 = 3.15(1) Å, O26–C12 = 3.03(3) Å, W1–C1 = 3.16(3) Å) (Figure 4b and Table S6). Additionally, thermogravimetric analysis (Figure 5b) indicated that relevant weight loss, occurring at temperatures higher than 100 °C (7% in weight), is due to the expulsion from the structure of extraframework ions embedded in the ZSM-5 channels. The residual one at lower temperature can be ascribed to the expulsion of water and/or CB molecules bonded to the surface (3% in weight below ~100 °C).

These results are quite well supported by the total amount of adsorbed molecules detected through both saturation capacity determined by the adsorption isotherm and the results obtained by Rietveld analysis. After adsorption, the T–O bond length ranges from 1.602 to 1.608 Å, the O–T–O angles varies from 96° to 125°, with a mean value of 109.4° (Table S6). According to Wragg et al. [44] the T–O–T bond angles adopt a wide range of values from 124° to 178° (Table S6). Regarding the channel geometry, after organics adsorption, any changes in both shape and channel dimension were also evaluated. Specifically, both straight and sinusoidal channels hosting the organic molecules change their shape and become more elliptical (Table 5).

Table 5. C.F.A. and ellipticity (ϵ) comparison between unloaded ZSM-5 [13] and ZSM-5–CB systems. C.F.A. = $\pi \cdot (\text{mean radius})^2$ (\AA^2); ϵ = ratio between the longest and the shortest pore dimensions.

Straight Channel						
O–O distance (\AA)	O7–O1	O8–O2	O31–O37	O44–O46	O47–O48	ϵ
ZSM-5–CB	8.22	8.20	8.02	8.22	7.97	1.03
ZSM-5	7.90	7.94	8.04	8.41	7.80	1.08
Free diameter (\AA)	O7–O1	O8–O2	O31–O37	O44–O46	O47–O48	
ZSM-5–CB	5.52	5.50	5.32	5.52	5.27	-
ZSM-5	5.20	5.24	5.34	5.71	5.10	-
	Mean diameter (\AA)	Mean radius (\AA)	C.F.A. (\AA^2)			
ZSM-5–CB	5.43	2.71	23.12	-		
ZSM-5	5.32	2.66	22.20	-		
O–O distance (\AA)	O11–O5	O20–O18	O21–O22	O27–O33	O28–O34	ϵ
ZSM-5–CB	8.08	7.89	8.11	8.22	8.08	1.04
ZSM-5	8.19	8.35	7.98	8.13	7.76	1.08
Free diameter (\AA)	O11–O5	O20–O18	O21–O22	O27–O33	O28–O34	
ZSM-5–CB	5.38	5.19	5.41	5.52	5.38	
ZSM-5	5.49	5.65	5.28	5.43	5.06	
	Mean diameter (\AA)	Mean radius (\AA)	C.F.A. (\AA^2)			
ZSM-5–CB	5.37	2.69	22.67			
ZSM-5	5.38	2.69	22.74			
Sinusoidal Channel						
O–O distance (\AA)	O20–O15	O24–O26	O27–O2	O28–O1	O41–O46	ϵ
ZSM-5–CB	8.08	7.87	7.76	8.16	8.69	1.12
ZSM-5	8.15	8.07	7.97	7.76	8.51	1.10
Free diameter (\AA)	O20–O15	O24–O26	O27–O2	O28–O1	O41–O46	
ZSM-5–CB	5.38	5.17	5.06	5.46	5.99	
ZSM-5	5.45	5.37	5.27	5.06	5.81	
	Mean diameter (\AA)	Mean radius (\AA)	C.F.A. (\AA^2)			
ZSM-5–CB	5.41	2.71	23.01			
ZSM-5	5.39	2.70	22.82			
O–O distance (\AA)	O17–O18	O23–O25	O30–O5	O31–O4	O44–O43	ϵ
ZSM-5–CB	7.50	8.58	8.20	7.89	7.75	1.14
ZSM-5	7.30	8.31	8.32	8.05	7.95	1.14
Free diameter (\AA)	O17–O18	O23–O25	O30–O5	O31–O4	O44–O43	
ZSM-5–CB	4.80	5.88	5.50	5.19	5.05	
ZSM-5	4.60	5.61	5.62	5.35	5.25	
	Mean diameter (\AA)	Mean radius (\AA)	C.F.A. (\AA^2)			
ZSM-5–CB	5.28	2.64	21.92			
ZSM-5	5.29	2.64	21.93			

4. Conclusions

This work aims to highlight the adsorptive capacity of commercial high silica zeolites ZSM-5 (MFI topology), and Y zeolite (FAU topology), for removal of chlorobenzene (CB) from water. Both high silica ZSM-5 and Y zeolites are characterized by fast kinetics, that combined with good adsorption capacity, suggest they can be efficiently used as a sorbent media to control the concentration of chlorobenzene in water systems. In particular, ZSM-5 is more efficient in the removal of CB at low concentration level, while Y shows higher saturation capacity than ZSM-5. Difference Fourier maps of the electron density provide insight into the preferred zeolite adsorption sites in both microporous materials. The refined framework–extraframework bond distances highlight the existence of CB, and hydrophobic zeolites interactions mediated via co-adsorbed H₂O molecules. Adsorption of CB on ZSM-5 and Y zeolites is accompanied by structural changes, i.e. variations in both unit-cell parameters and channel shape when compared to the as-synthesized microporous materials, clearly confirming the very relevant role of H₂O molecules in both the diffusion and adsorption processes in hydrophobic zeolites. After adsorption, the channels become more distorted, thus indicating remarkable framework flexibility for both ZSM-5 and Y zeolites.

Supplementary Materials: The following are available online at www.mdpi.com/2075-163x/8/3/80/s1, Figure S1: Observed (dotted line), calculated (solid line) and difference (bottom) X-ray powder diffraction patterns of Y–CB (a) and ZSM-5–CB (b), respectively, Table S1: Framework atomic fractional coordinates and thermal isotropic displacement factor of Y–CB, Table S2: Framework atomic fractional coordinates and thermal isotropic displacement factor of ZSM-5–CB, Table S3: Extraframework atomic fractional coordinates, thermal isotropic displacement factor and occupancy of Y–CB, Table S4: Extraframework atomic fractional coordinates, thermal isotropic displacement factor and occupancy of ZSM-5–CB; x/a atomic fractional coordinates of CB2 molecule atoms have exactly the same values, in order to maintain the molecule planarity, Table S5: Selected bond distances (Å) and angles (°) within both the Y–CB framework and extraframework atoms at T_{amb} , Table S6: Selected bond distances (Å) and angles (°) within both the ZSM-5–CB framework and extraframework atoms at T_{amb} . CIFs for all reported crystal structures are added as Supplementary Information.

Acknowledgments: The authors thank the Italian University and Scientific Research Ministry (Grant PRIN Prot. 2015HK93L7), the Istituto ENI Donegani-Environmental Technologies (Novara, Italy) and the Laboratory Terra&Acqua Tech, Technopole of Ferrara of Emilia-Romagna High Technology Network for their financial support.

Author Contributions: The manuscript was written with contributions from all authors. All authors have given approval to the final version of the manuscript. Annalisa Martucci wrote the paper and performed the X-ray and chromatographic experiments with Luisa Pasti; Elisa Rodeghero, Giada Beltrami and Matteo Ardit conceived and designed the XRD experiments and analyzed the data; Elena Sarti, Tatiana Chenet and Claudia Stevanin conceived and designed the adsorption experiments and analyzed the data.

Conflicts of Interest: The authors declare no conflict of interest.

References

1. Sennour, R.; Mimane, G.; Benghalem, A.; Taleb, S. Removal of the persistent pollutant chlorobenzene by adsorption onto activated montmorillonite. *Appl. Clay Sci.* **2009**, *43*, 503–506. [[CrossRef](#)]
2. McClenny, W.A.; Oliver, K.D.; Jacumin, H.H., Jr.; Daughtrey, E.H., Jr. Ambient level volatile organic compound (VOC) monitoring using solid adsorbents—Recent US EPA studies. *J. Environ. Monitor.* **2002**, *4*, 695–705. [[CrossRef](#)]
3. Khan, F.I.; Ghoshal, A.K. Removal of Volatile Organic Compounds from polluted air. *J. Prevent. Proc.* **2000**, *13*, 527–545. [[CrossRef](#)]
4. Sarti, E.; Chenet, T.; Pasti, L.; Cavazzini, A.; Rodeghero, E.; Martucci, A. Effect of silica alumina ratio and thermal treatment of beta zeolites on the adsorption of toluene from aqueous solutions. *Minerals* **2017**, *7*, 22. [[CrossRef](#)]
5. Rodeghero, E.; Pasti, L.; Sarti, E.; Cruciani, G.; Bagatin, R.; Martucci, A. Temperature-induced desorption of methyl tert-butyl ether confined on ZSM-5: An in situ synchrotron XRD powder diffraction study. *Minerals* **2017**, *7*, 34. [[CrossRef](#)]

6. Rodeghero, E.; Martucci, A.; Cruciani, G.; Bagatin, R.; Sarti, E.; Bosi, V.; Pasti, L. Kinetics and dynamic behaviour of toluene desorption from ZSM-5 using in situ high-temperature synchrotron powder X-ray diffraction and chromatographic techniques. *Catal. Today* **2016**, *227*, 118–125. [[CrossRef](#)]
7. Arletti, R.; Martucci, A.; Alberti, A.; Pasti, L.; Nassi, M.; Bagatin, R. Location of MTBE and toluene in the channel system of the zeolite mordenite: Adsorption and host–guest interactions. *J. Solid State Chem.* **2012**, *194*, 135–142. [[CrossRef](#)]
8. Pasti, L.; Rodeghero, E.; Sarti, E.; Bosi, V.; Cavazzini, A.; Bagatin, R.; Martucci, A. Competitive adsorption of VOCs from binary aqueous mixtures on zeolite ZSM-5. *RSC Adv.* **2016**, *6*, 54544–54552. [[CrossRef](#)]
9. Pasti, L.; Sarti, E.; Cavazzini, A.; Marchetti, N.; Dondi, F.; Martucci, A. Factors affecting drug adsorption on beta zeolites. *J. Sep. Sci.* **2013**, *36*, 1604–1611. [[CrossRef](#)] [[PubMed](#)]
10. Martucci, A.; Pasti, L.; Marchetti, N.; Cavazzini, A.; Dondi, F.; Alberti, A. Adsorption of pharmaceuticals from aqueous solutions on synthetic zeolites. *Micropor. Mesopor. Mat.* **2012**, *148*, 174–183. [[CrossRef](#)]
11. Braschi, I.; Blasioli, S.; Gigli, L.; Gessa, C.E.; Alberti, A.; Martucci, A. Removal of sulfonamide antibiotics from water: Evidence of adsorption into an organophilic zeolite Y by its structural modifications. *J. Hazard. Mater.* **2010**, *17*, 218–225. [[CrossRef](#)] [[PubMed](#)]
12. Blasioli, S.; Martucci, A.; Paul, G.; Gigli, L.; Cossi, M.; Johnston, C.T.; Marchese, L.; Braschi, I. Removal of sulfamethoxazole sulfonamide antibiotic from water by high silica zeolites: A study of the involved host–guest interactions by a combined structural, spectroscopic, and computational approach. *J. Colloid Interf. Sci.* **2014**, *419*, 148–159. [[CrossRef](#)] [[PubMed](#)]
13. Pasti, L.; Martucci, A.; Nassi, M.; Cavazzini, A.; Alberti, A.; Bagatin, R. The role of water in DCE adsorption from aqueous solutions onto hydrophobic zeolites. *Micropor. Mesopor. Mat.* **2012**, *160*, 182–193. [[CrossRef](#)]
14. Guo, Y.; Li, Y.; Zhu, T.; Ye, M.; Wang, X. Adsorption of SO₂ and chlorobenzene on activated carbon. *Adsorpt.* **2013**, *19*, 1109–1116. [[CrossRef](#)]
15. Crisafulli, R.; Milhome, M.A.L.; Cavalcante, R.M.; Silveira, E.R.; De Keukeleire, D.; Nascimento, R.F. Removal of some polycyclic aromatic hydrocarbons from petrochemical wastewater using low-cost adsorbents of natural origin. *Bioresour. Technol.* **2008**, *99*, 4515–4519. [[CrossRef](#)] [[PubMed](#)]
16. Kim, B.K.; Ryu, S.K.; Kim, B.J.; Park, S.J. Roles of Acid-Base Interactions in Hydrogen Chloride Removal by Activated Carbon Fibers. *J. Ind. Eng. Chem.* **2006**, *12*, 121–126.
17. Park, S.J.; Kim, B.J. Influence of oxygen plasma treatment on hydrogen chloride removal of activated carbon fibers. *J. Colloid Interf. Sci.* **2004**, *275*, 590–595. [[CrossRef](#)] [[PubMed](#)]
18. Chin, C.J.M.; Shih, M.W.; Tsai, H.J. Adsorption of nonpolar benzene derivatives on single-walled carbon nanotubes. *Appl. Surf. Sci.* **2010**, *256*, 6035–6039. [[CrossRef](#)]
19. Long, C.; Li, Q.; Li, Y.; Liu, Y.; Li, A.; Zhang, Q. Adsorption characteristics of benzene–chlorobenzene vapor on hypercrosslinked polystyrene adsorbent and a pilot-scale application study. *Chem. Eng. J.* **2010**, *160*, 723–728. [[CrossRef](#)]
20. Chen, W.; Duan, L.; Zhu, D. Adsorption of polar and nonpolar organic chemicals to carbon nanotubes. *Environ. Sci. Technol.* **2007**, *41*, 8295–8300. [[CrossRef](#)] [[PubMed](#)]
21. Balamurugan, K.; Subramanian, V. Adsorption of chlorobenzene onto (5,5) armchair single-walled Carbon nanotube and graphene sheet: Toxicity versus adsorption strength. *J. Phys. Chem. C* **2013**, *117*, 21217–21227. [[CrossRef](#)]
22. Lee, J.J.; Choi, J.; Park, J.W. Simultaneous sorption of lead and chlorobenzene by organobentonite. *Chemosphere* **2002**, *49*, 1309–1315. [[CrossRef](#)]
23. Witthuhn, B.; Klauth, P.; Pernyeszi, T.; Vereecken, H.; Klumpp, E. Organoclays for Aquifer Bioremediation: Adsorption of Chlorobenzene on Organoclays and its Degradation by RHODOCOCCUS B528. *Water Air Soil Poll. Focus* **2006**, *6*, 317–329. [[CrossRef](#)]
24. Jarraya, I.; Fourmentin, S.; Benzina, M.; Bouaziz, S. VOC adsorption on raw and modified clay materials. *Chem. Geol.* **2010**, *275*, 1–8. [[CrossRef](#)]
25. Altare, C.R.; Bowman, R.S.; Katz, L.E.; Kinney, K.A.; Sullivan, E.J. Regeneration and long-term stability of surfactant-modified zeolite for removal of volatile organic compounds from produced water. *Micropor. Mesopor. Mat.* **2007**, *105*, 305–316. [[CrossRef](#)]
26. Anderson, M.A. Removal of MTBE and Other Organic Contaminants from Water by Sorption to High Silica Zeolites. *Environ. Sci. Technol.* **2000**, *34*, 725–727. [[CrossRef](#)]

27. Damjanović, L.; Rakić, V.; Rac, V.; Stošić, D.; Auroux, A. The investigation of phenol removal from aqueous solutions by zeolites as solid adsorbents. *J. Hazard. Mat.* **2010**, *184*, 477–484. [[CrossRef](#)] [[PubMed](#)]
28. Perego, C.; Bagatin, R.; Tagliabue, M.; Vignola, R. Zeolites and related mesoporous materials for multi-talented environmental solutions. *Micropor. Mesopor. Mat.* **2013**, *166*, 37–49. [[CrossRef](#)]
29. Leardini, L.; Martucci, A.; Braschi, I.; Blasioli, S.; Quartieri, S. Regeneration of high-silica zeolites after sulfamethoxazole antibiotic adsorption: A combined in situ high-temperature synchrotron X-ray powder diffraction and thermal degradation study. *Mineral. Mag.* **2014**, *78*, 1141–1160. [[CrossRef](#)]
30. Braschi, I.; Blasioli, S.; Buscaroli, E.; Montecchio, D.; Martucci, A. Physicochemical regeneration of high silica zeolite Y used to clean-up water polluted with sulfonamide antibiotics. *J. Environ. Sci.* **2016**, *43*, 302–312. [[CrossRef](#)] [[PubMed](#)]
31. Vignola, R.; Cova, U.; Fabiani, F.; Sardellati, T.; Sisto, R.; Vignola, R. Process for the regeneration of nonpolar adsorbing zeolites used for the treatment of contaminated water. Patent WO/2009/000429, 31 December 2008.
32. Alberti, A.; Martucci, A. Phase transformations and structural modifications induced by heating in microporous materials. *Stud. Surf. Sci. Catal.* **2005**, *155*, 19–43. [[CrossRef](#)]
33. Alberti, A.; Martucci, A. Reconstructive phase transitions in microporous materials: Rules and factors affecting them. *Micropor. Mesopor. Mat.* **2011**, *141*, 192–198. [[CrossRef](#)]
34. Baerlocher, C.; McCusker, L.B.; Olson, D.H. *Atlas of Zeolite Framework Types*, 6th ed.; Elsevier: Amsterdam, The Netherlands, 2007.
35. Larson, A.C.; Von Dreele, R.B. *GSAS General Structure Analysis System, LANSCE, MS-H805*; Los Alamos National Laboratory: Los Alamos, NM, USA, 1994.
36. Toby, B.H. EXPGUI, a graphical user interface for GSAS. *J. Appl. Crystallogr.* **2001**, *34*, 210–213. [[CrossRef](#)]
37. Azizian, S.; Haerifar, M.; Bashiri, H. Adsorption of methyl violet onto granular activated carbon: Equilibrium, kinetics and modeling. *Chem. Eng. J.* **2009**, *146*, 36–41. [[CrossRef](#)]
38. De Moor, B.A.; Reyniers, M.F.; Gobin, O.C.; Lercher, J.A.; Marin, G.B. Adsorption of C2–C8 *n*-Alkanes in Zeolites. *J. Phys. Chem. C* **2011**, *115*, 1204–1219. [[CrossRef](#)]
39. Martucci, A.; Braschi, I.; Bisio, C.; Sarti, E.; Rodeghero, E.; Bagatin, R.; Pasti, L. Influence of water on the retention of methyl tertiary-butyl ether by high silica ZSM-5 and Y zeolites: A multidisciplinary study on the adsorption from liquid and gas phase. *RSC Advances* **2015**, *5*, 86997–87006. [[CrossRef](#)]
40. Martucci, A.; Braschi, I.; Marchese, L.; Quartieri, S. Recent advances in clean-up strategies of waters polluted with sulfonamide antibiotics: A review of sorbents and related properties. *Mineral. Mag.* **2014**, *78*, 1115–1140. [[CrossRef](#)]
41. Li, X.; Chen, G.H. Surface modified graphite nanosheets used as adsorbent to remove 1,2-dichlorobenzene from water. *Mater. Lett.* **2009**, *63*, 930–932. [[CrossRef](#)]
42. Yu, F.; Ma, J.; Wu, Y. Adsorption of toluene, ethylbenzene and *m*-xylene on multi-walled carbon nanotubes with different oxygen contents from aqueous solutions. *J. Hazard. Mater.* **2011**, *192*, 1370–1379. [[CrossRef](#)] [[PubMed](#)]
43. Krishna, R.; van Baten, J.M. Highlighting a Variety of Unusual Characteristics of Adsorption and Diffusion in Microporous Materials Induced by Clustering of Guest Molecules. *Langmuir* **2010**, *26*, 8450–8463. [[CrossRef](#)] [[PubMed](#)]
44. Wragg, D.S.; Morris, R.E.; Burton, A.W. Pure silica zeolite-type frameworks: A structural analysis. *Chem. Mater.* **2008**, *20*, 1561–1570. [[CrossRef](#)]
45. Leardini, L.; Martucci, A.; Alberti, A.; Cruciani, G. Template burning effects on stability and boron coordination in boron lewyne studied by in situ time resolved synchrotron powder diffraction. *Micropor. Mesopor. Mater.* **2013**, *167*, 117–126. [[CrossRef](#)]
46. Baur, W.H. Self-limiting distortion by antirotating hinges is the principle of flexible but noncollapsible frameworks. *J. Solid State Chem.* **1992**, *97*, 243–247. [[CrossRef](#)]
47. Momma, K.; Izumi, F. VESTA 3 for three-dimensional visualization of crystal, volumetric and morphology data. *J. Appl. Crystallogr.* **2011**, *44*, 1272–1276. [[CrossRef](#)]

